sustainability

MDPI

Article

A Novel FCS-MPC Method of Multi-Level APF Is Proposed to Improve the Power Quality in Renewable Energy Generation Connected to the Grid

Hong Li *, Yang Liu * and Jianfeng Yang

School of Automation and Electrical Engineering, Lanzhou Jiaotong University, Lanzhou 730070, China; jfyang@mail.lzjtu.cn

* Correspondence: hong_0927@163.com (H.L.); yang.lts@foxmail.com (Y.L.); Tel.: +86-139-1986-1616 (H.L.); +86-181-8953-2293 (Y.L.)

Abstract: When photovoltaic, wind, energy storage batteries, and other new forms of energy are connected to the grid, power electronic converters are needed, and there are a lot of nonlinear devices in the grid. The characteristics of sustainable energy generation determine the variability and intermittency, which will produce harmonic components. Active power filters (APF) are commonly used in industry for harmonic compensation, so it is of great significance to control APF quickly and effectively. The multi-objective, single-factor, multistep finite control set model predictive control (FCS-MPC) of an APF proposed in this paper is suitable for a multi-objective, multi-level converter control. This method is applied to the three-level APF structure, which changes the traditional three-level FCS-MPC control method. The traditional three-level FCS-MPC includes four control objectives, stable control of the DC-side voltage, power grid harmonic currents generated under non-linear loads, and balance of the capacitor voltage on the DC side when switching frequency. This method uses the redundant switching state of the three-level structure to achieve the voltage balance of the two capacitors on the DC side, which reduces the difficulty of target optimisation caused by the selection of weight factors. Based on the multi-step prediction, power feedback control is added on the DC side to increase the DC side's reaction speed, eliminate the influence of uncertainty, and realise better dynamic performance. According to the simulation results, we can observe that the proposed method has good followability, can compensate for the harmonics of the power grid, reduces the harmonic content to less than 5%, and can balance the DC-side capacitor voltage.

Keywords: active power filter; finite control set model predictive control; power feedback control; balance of capacitor voltage

check for updates

Citation: Li, H.; Liu, Y.; Yang, J. A Novel FCS-MPC Method of Multi-Level APF Is Proposed to Improve the Power Quality in Renewable Energy Generation Connected to the Grid. *Sustainability* **2021**, *13*, 4094. https://doi.org/10.3390/su13084094

Academic Editor: Mohamed Abdelrahem

Received: 10 March 2021
Accepted: 4 April 2021
Published: 7 April 2021

Publisher's Note: MDPI stays neutral with regard to jurisdictional claims in published maps and institutional affiliations.

Copyright: © 2021 by the authors. Licensee MDPI, Basel, Switzerland. This article is an open access article distributed under the terms and conditions of the Creative Commons Attribution (CC BY) license (https://creativecommons.org/licenses/by/4.0/).

1. Introduction

The application of grid-connected technology can convert solar energy and wind energy into electric energy resources to meet energy demand and realise the rapid development of the power grid [1]. However, in the specific application process of grid-connected technology, the general control mode is not suitable for the obvious voltage, and current harmonics can easily appear in the process of grid connection. The grid connection is also affected by the lighting, angle, wind speed, and other factors, which increase the harmonic pollution of the power system [2]. The integration of new energy leads to the diversification of energy, but it affects the power quality of the power system to a certain extent, so there are certain security threats in the operation of the power system, and there are many hidden dangers of power accidents. If it is serious, it will even lead to the paralysis of the entire power system and affect people's normal production and life. Necessary measures must be taken to improve the application efficiency of new energy integration, such as active power filters (APF). An APF is a device that can compensate for both harmonic and reactive power. The principle of APF is to inject the detected harmonics

in a reverse direction to achieve the purpose of harmonic cancellation [3]. Since APF was put forward, many control methods have appeared, including proportional integral (PI) control, which is widely used in traditional industry. However, with the PI control method, it is difficult to achieve multi-objective control, and the parameter tuning is difficult to adjust. It has a certain lag through the error feedback adjustment at the current moment, and the industrial environment has a certain variability, so it is difficult to adjust the PI parameters in real time [4,5].

Due to the transformation between AC and DC and the intermittent renewable sources in the power grid, researchers [6] have proposed a metaheuristic-based vector-decoupled algorithm to balance the control and operation of hybrid microgrids in the presence of stochastic renewable energy sources and electric vehicles' charging structures. It ensures the stability of the voltage and frequency level under the harsh conditions of island operation and high pulse demand, as well as the variability of the renewable energy production, in order to improve the power quality of renewable energy. The literature [7] has proposed a hybrid fuzzy back-propagation control scheme for a unified power quality conditioner (UPQC). The reference current of the controller is controlled by the inverse propagation algorithm, and the reference voltage of the controller is controlled by fuzzy logic, which effectively improves the power quality. The literature [8] has also proposed a single-phase unified power quality conditioner based on a modular multilevel matrix converter (M3C). In this topology, DC circulating current is used to balance the instantaneous active power of each arm, to prevent voltage divergence between the arms and within the arms, to realise voltage balance between the capacitors.

Model predictive control (MPC) is a control method developed from practice to theory with the participation of industry, and includes dynamic matrix control (DMC), model algorithm control (MAC), and generalised predictive control (GPC). With the development of microprocessors, MPC has been widely used in power electronics and converters. General power electronic devices have strong nonlinearity and a limited switching state [9,10]. Rodriguez et al. proposed the finite set model predictive control (FCS-MPC) [11] using the value function to select the optimal switch combination. However, the problem with traditional FCS-MPC is online calculation, and the switching frequency is not fixed [12,13].

Concerning the problems that existed in the control method of FCS-MPC, many scholars in related fields have proposed different methods [14]. Studies [15] have considered an MPC method with time-delay compensation. The reference current is predicted by Lagrange' interpolation. In the future, multiple prediction periods will be calculated. Due to the irregular and rapid variation of harmonics, the prediction corresponding to the predicted reference value has a large error at the change. Previous work [16] has pointed out that FCS-MPC was applied to APF to compensate for the harmonic current and reactive power.

In the traditional FCS-MPC method of the three-level converter, it is necessary to perform a weighted control on multiple objectives. In [17], which synthesises voltage vectors with different duty cycles, a multi-objective optimisation strategy is used to find the best duty cycle to balance the capacitor voltage on the DC side. The algorithm has the problem of extensive computation. In order to simplify the selection of the multi-level weighting factors in a photovoltaic grid connection, researchers [18] proposed a search scheme to divide the traditional FCS-MPC into three steps to achieve the optimal control of each step, which is ineffective in solving the FCS-MPC delay problem. The literature [14] proposed an FCS-MPC control method using a redundant switching state; however, because of the high sampling frequency and time-delay of FCS-MPC, it cannot provide better compensation and resulting performance. The method proposed in this paper improves the power quality of a power grid, improves the compensation performance of APF by using a multi-level structure, avoids the multi-weight factor selection of the multi-step FCS-MPC algorithm, and further improves the control effect by using multi-step prediction.

In this paper, a multi-step prediction based on a single weighting factor is proposed, and a power feedforward control method is proposed to accelerate the dynamic charac-

teristics of APF and the stability of the DC side. The FCS-MPC with a redundant switch combination omits the selection of the weight coefficients in the case of the DC-side capacitor balance in the three-level APF, and the use of redundant vectors has different effects on the capacitor voltage without changing the output so that the selection of the optimal switching state can completely follow the harmonic reference current. It is difficult to balance the optimisation of many objectives and select a weighting factor. If there are too many objectives, the calculation time will increase, and the control effect will be delayed. The problem of how to accomplish the optimisation of these control objectives is the selection of the weight factors, and limiting their use can reduce the calculation of the system and improve the response speed.

In this paper, a simulation model of the entire system is established and compared with the multi-step, multi-weight factor control method to verify the superiority of the single-factor control method under a power feedforward in a multi-level APF [18,19]. The structure of this paper includes six parts: the second section introduces the three-phase NPC-APF model and the harmonic current detection method [19]; the third section introduces the FCS-MPC; the fourth section introduces the NPC-APF under a single weight factor; and the fifth section shows the performance and results of the multi-step FCS-MPC control method through simulation results. The sixth part is the conclusion.

2. Mathematical Model of Three-Phase Parallel APF

Figure 1 shows the structure of the NPC-type three-level APF [20]. e_a, e_b, and e_c are the power grid voltages. i_{La}, i_{Lb}, and i_{Lc} are the currents on the load side of the grid. i_{Ca}, i_{Cb}, and i_{Cc} are the compensation currents of APF, and R and L are the filter inductance and resistance, respectively. In the NPC-type APF, each phase is composed of two diodes and four (Insulated Gate Bipolar Transistor) IGBT devices. The midpoint of the two diodes is connected to the midpoint of the DC side. The DC side is composed of capacitors C_1 and C_2. The voltages of C_1 and C_2 need to be controlled in a relatively balanced fashion.

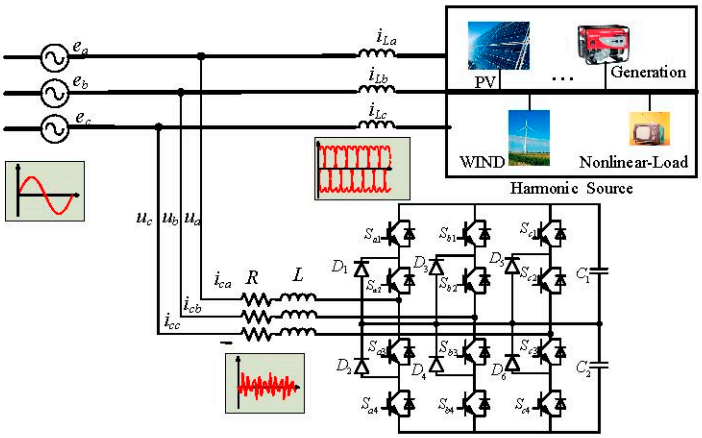


Figure 1. Three-phase parallel NPC-type three-level APF structure diagram.

2.1. Operating Principle of Three-Level APF

For a three-level APF, each bridge arm consists of four IGBTs, and there can be a total of 27 different switching state combinations. Each bridge arm is defined as three states of P, 0, and N in Equation (1), which correspond to three outputs.

$$S_x = \begin{cases} P\ S_{x1} = S_{x2} = 1, S_{x3} = S_{x4} = 0; \\ 0\ \ S_{x1} = S_{x4} = 0, S_{x2} = S_{x3} = 1; \\ N\ S_{x1} = S_{x2} = 0, S_{x3} = S_{x4} = 1; \end{cases} \quad (1)$$

where $x = a, b, c$ represents three bridge arms; and S_{x1}, S_{x2}, S_{x3}, and S_{x4} are the switches of each IGBT. These 27 switching states can generate 19 types of vectors, including three

sets of zero vectors and 12 sets of redundant vectors. The 27 switch states and redundant vectors are shown in Figure 2 [20].

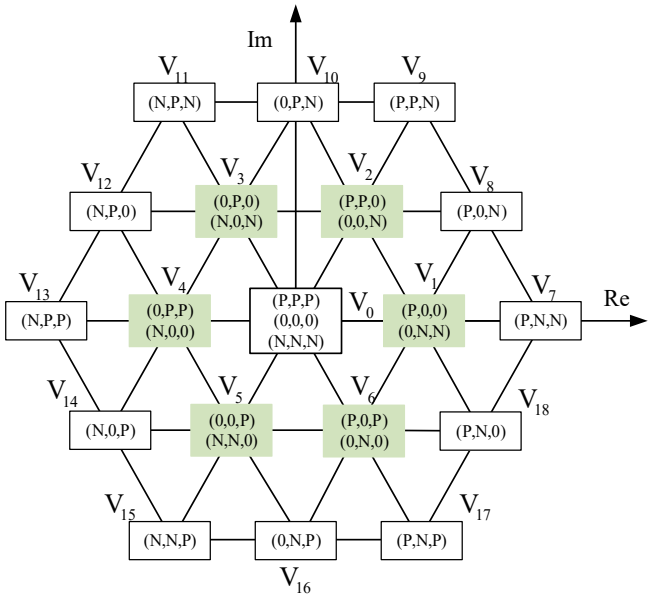


Figure 2. Switch state and voltage vector.

Among them, V_1 to V_6 are the voltage vectors composed of two sets of different switch states, each containing redundant switch states. V_0 contains three sets of zero vectors: (0, 0, 0), (P, P, P), and (N, N, N). According to the voltage switch state, the vector output can be obtained as (2). There are three groups of bridge arms that determine the output voltage.

$$u_{out} = \frac{2}{3}\left(\frac{U_{dc}}{2}S_a + \alpha S_b\frac{U_{dc}}{2} + \alpha^2 S_c\frac{U_{dc}}{2}\right) \tag{2}$$

where

$$\alpha = e^{j2\pi/3} = -\frac{1}{2} + j\frac{\sqrt{3}}{2}$$

2.2. Mathematical Model of APF

The FCS-MPC of the current will cause errors when tracking under a sinusoidal signal. The higher the frequency, the greater the error; therefore, the collected reference signal is outputted in the α-β coordinate system after the prediction model is outputted, and APF performs tracking reference prediction. The signal can be convenient and intuitive. If the grid voltage were balanced, according to Kirchhoff's current law, the APF output currents i_a, i_b, i_c; the grid voltages e_a, e_b, e_c; and the output voltages u_a, u_b, u_c would converted to α-β with Equation (3).

$$\begin{bmatrix} i_{c\alpha} \\ i_{c\beta} \end{bmatrix} = C_{32}\begin{bmatrix} i_{ca} \\ i_{cb} \\ i_{cc} \end{bmatrix}, \begin{bmatrix} e_\alpha \\ e_\beta \end{bmatrix} = C_{32}\begin{bmatrix} e_a \\ e_b \\ e_c \end{bmatrix}, \begin{bmatrix} u_\alpha \\ u_\beta \end{bmatrix} = C_{32}\begin{bmatrix} u_a \\ u_b \\ u_c \end{bmatrix} \tag{3}$$

where

$$C_{32} = \sqrt{\frac{2}{3}}\begin{bmatrix} 1 & -\frac{1}{2} & \frac{1}{2} \\ 0 & \frac{\sqrt{3}}{2} & -\frac{\sqrt{3}}{2} \end{bmatrix}$$

In the α-β coordinate system, the mathematical model of the α-β axis of the APF can be obtained as

$$\begin{bmatrix} \frac{di_{c\alpha}}{dt} \\ \frac{di_{c\beta}}{dt} \end{bmatrix} = \begin{bmatrix} -\frac{R}{L} & 0 \\ -0 & -\frac{R}{L} \end{bmatrix} \begin{bmatrix} i_{c\alpha} \\ i_{c\beta} \end{bmatrix} + \begin{bmatrix} \frac{1}{L} & 0 \\ 0 & \frac{1}{L} \end{bmatrix} \begin{bmatrix} e_\alpha - u_\alpha \\ e_\beta - u_\beta \end{bmatrix} \quad (4)$$

2.3. i_p-i_q Harmonic Detection Method

The harmonic detection of APF is mainly based on the i_p-i_q method of instantaneous reactive power theory, which extracts the distorted current harmonics from the three-phase load current [21]. The specific principle diagram is shown in Figure 3. If the load currents i_{La}, $i_{Lb,}$ and i_{Lc} are changed to the d-q coordinate system and pass the low-pass filter (LPF), only the fundamental current remains, and then inversely transforms to the a, b, c coordinate system. Only the residual harmonic current (the load current minus the fundamental current) is compensated as the command current to the APF. The PI controller is used to obtain the DC-side reference current to make it stable at the reference voltage setting.

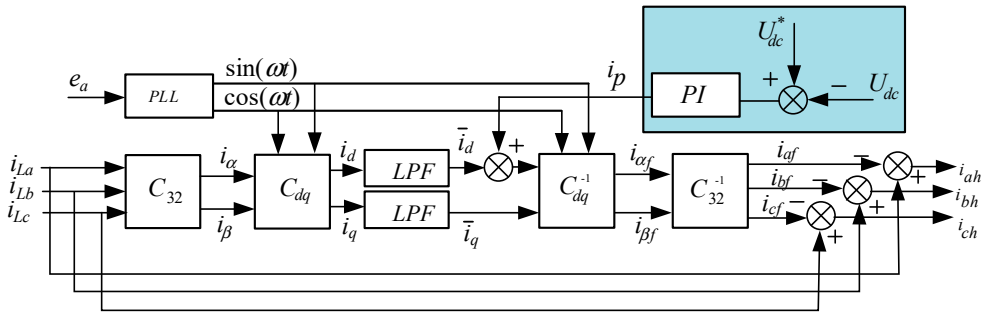


Figure 3. Block diagram of the three-phase i_p-i_q harmonic detection.

where

$$C_{dq} = \begin{bmatrix} \sin\omega t & -\cos\omega t \\ -\cos\omega t & -\sin\omega t \end{bmatrix} \quad (5)$$

3. FCS-MPC of Three-Level APF

As shown in Figure 2, in the α-β coordinate system, $V_{x(x=0,1,\ldots,7)}$ is the 27 voltage vectors, while $J_{\min}$ is the voltage vector with the smallest objective function. To get the switching signal combination state to directly control the APF output, take the tracking principle of the FCS-MPC algorithm at a certain sampling moment, calculate the cost function by comprehensively switching the frequency, the tracking error, and so on, and seek to obtain the optimal target.

3.1. APF Control Principle

The principle diagram of APF's current predictive control is shown in Figure 4. The harmonic source is replaced by a nonlinear load. i_o is the predicted active current component value of APF, and $i^*(k)$ is the existing harmonic reference current. Generally, the difference between the DC side and the reference value is used. In this paper, the power control is performed on the DC side, the voltage regulator is controlled by the PI regulator, and the compensation is performed together with the harmonics [22]. After the objective function, the optimal switch combination is directly applied to the APF to control the APF's output compensation current to track the harmonics at the current moment and predict the next time reference signal.

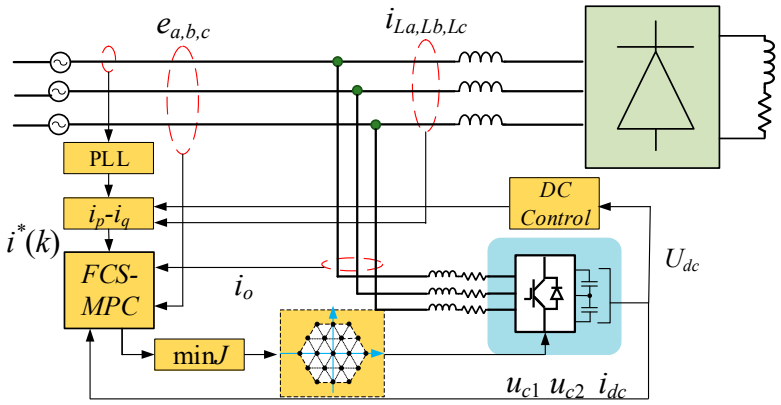


Figure 4. APF predictive control principle.

3.2. Power Feedback Control

The principle diagram of FCS-MPC for the power feedforward control is shown in Figure 5. Compared with the traditional direct current PI adjustment, power feedforward control directly adjusts the PI power on the DC side. After proportional signal amplification, the dynamic performance of the DC-side voltage regulator control is improved.

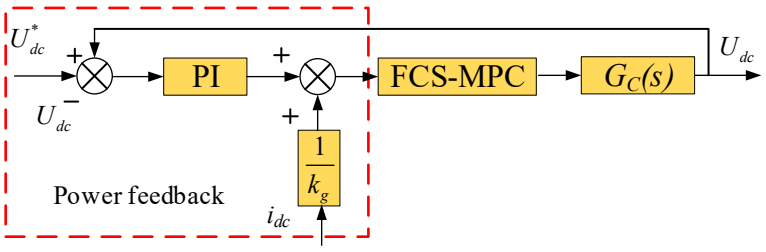


Figure 5. The control structure of DC bus voltage.

In the figure above, $G_C(s)$ is the current closed-loop transfer function, and U^* is the reference value of the DC-side voltage. U is the current voltage value of the DC side, i_{dc} is the current value of DC side, and k_g is the gain coefficient.

4. Single-Step FCS-MPC of Traditional NPC Converter

The two capacitors C_1 and C_2 on the DC side are dynamically modelled and described by the difference Equation (6), where the capacitance values of C_1 and C_2 are equal, C is the value of C_1 and C_2, u_{c1} and u_{c2} are the voltage values of the capacitors, and i_{c1} and i_{c2} are the current values of the two capacitors.

$$\begin{cases} \frac{du_{c1}}{dt} = \frac{1}{C} i_{c1} \\ \frac{du_{c2}}{dt} = \frac{1}{C} i_{c2} \end{cases} \tag{6}$$

Equation (6) performs differential discretisation to obtain Equation (7).

$$\frac{du_{cx}}{dt} = \frac{u_{cx}(k+1) - u_{cx}(k)}{T_s} \quad x = 1, 2 \tag{7}$$

Substituting Equation (7) into Equation (6) yields Equation (8). Equation (8) is a discrete equation after the Euler forward difference, which can predict the next moment.

$$\begin{cases} u^p_{c1}(k+1) = \frac{1}{C} i_{c1}(k) T_s + u_{c1}(k) \\ u^p_{c2}(k+1) = \frac{1}{C} i_{c2}(k) T_s + u_{c2}(k) \end{cases} \tag{8}$$

Among them, $i_{c1}(k)$ and $i_{c2}(k)$ are the current values determined by the switch and the output current, which is specifically determined by Equation (9).

$$\begin{cases} i_{c1}(k) = i_{dc}(k) - G_{1a}i_a(k) - G_{1b}i_b(k) - G_{1c}i_c(k) \\ i_{c2}(k) = i_{dc}(k) + G_{2a}i_a(k) + G_{2b}i_b(k) + G_{2c}i_c(k) \end{cases} \tag{9}$$

where $i_{dc}(k)$ is the DC-side current at time k; $i_a(k)$, $i_b(k)$, and $i_c(k)$ are the three-phase output currents at time k; and G_{1x} and G_{2x} are determined by the inverter's switching state at the current time, as per Equation (10).

$$G_{1x} = \begin{cases} 1, S_x = P \\ 0, others \end{cases}, G_{2x} = \begin{cases} 1, S_x = N \\ 0, others \end{cases}, x = a, b, c \tag{10}$$

A dynamic discrete model, Equation (11), is established for the APF system to predict the current output at the next moment.

$$i_o^p(k+1) = \frac{T_s}{L}(u_{out}(k) - e(k)) + (1 - \frac{RT_s}{L})i_o(k) \tag{11}$$

$i_o^p(k+1)$ is the predicted output current at the next moment; L is the filter inductance; R is the equivalent resistance; $i_o(k)$ is the current output value at the present moment k; and $u_{out}(k)$ is the voltage determined by the switch state. The value is determined by Equation (2). $e(k+1)$ is the grid-side voltage, and it does not change much in the adjacent sampling points, so $e(k+1) = e(k)$. The objective function of Equation (12) can be established.

$$J = \|i_\alpha^* - i_\alpha^p\|_{\lambda_1} + \|i_\beta^* - i_\beta^p\|_{\lambda_2} + \|u_{c1}^p - u_{c2}^p\|_{\lambda_3} + h_{\lim}(i) + \gamma_i s^2(i) \tag{12}$$

where

$$h_{\lim}(i) = \begin{cases} 0, \text{if} i_o^p(k+1) \le i_{\max} \\ \infty, \text{if} i_o^p(k+1) > i_{\max} \end{cases}$$

$$s(i) = \sum \left| i_{a,b,c}(k+1) - i_{a,b,c}(k) \right|$$

In the α-β coordinate system, *ih* α and *ih* β are the reference currents, *ip* α and *ip* β are the predicted outputs, and *up* $c1$ and *up* $c2$ are the predicted values of the capacitor voltage, making them equal by the weighting factors λ_1, λ_2, λ_3, and γ_i.

5. Multi-Step without Weight Factors FCS-MPC

5.1. Multi-Step Predictive

In a very small sampling period, T_s is very small, so the term *RTs* in Equation (11) can be ignored. The grid voltage e($k+1$) and the reference current $i^*(k+1)$ need to be estimated. With Lagrange's interpolation method (Equation (13)), the reference current using the prediction method to obtain the grid voltage and the reference current at the next moment are usually taken as the second or third order. For accuracy, the third-order interpolation is used, as shown in the following Equation (14). Similarly, the reference value at $k+2$ can also be obtained.

$$i^*(k+1) = \sum_{i=0}^{n} (-1)^{n-i} \frac{(n+1)!}{i!(n+1-i)!} \cdot i^*(k+i-n\ ) \tag{13}$$

$$i^*(k+1) = 4i^*(k) - 6i^*(k-1) + 4i^*(k-2\ ) - i^*(k-3) \tag{14}$$

Due to the conservative problem of a single-step FCS-MPC, which affects the compensation performance of the APF, this paper makes the calculation of the optimal state at the next moment of the two optimal control states generated by the objective function at the sampling moment.

The prediction output of the APF at the next moment from the single-step prediction is $i_o^p(k+1)$. The optimal two switch states $S_{\text{opt1}}(k+1)$ and $S_{\text{opt2}}(k+1)$ are obtained according

to the optimal solution of the objective function, and the obtained two switch states are applied to Equation (11). $i_p(k+1)$ and $v(k+1)$ are obtained, and Equation (11) is subjected to backward difference to obtain Equation (15). In Equation (15), the two optimal states $i_1^p(k+1)$ and $i_2^p(k+1)$ produced by single-step predictive control continue to predict the output.

$$i_o^p(k+2) = \frac{T_s}{L}(u_o(k+1) - e\,(k+1)) + \left(1 - \frac{RT_s}{L}\right) \cdot i_x^p(k+1) \;\; x = 1,2 \tag{15}$$

5.2. Single Objective

There are six sets of redundant vectors in the three-level APF. Each of these six sets of redundant vectors produces the same output voltage in the APF, but has different effects on the current at the midpoint of the DC side. Thus, it has different effects on the voltage trend of the two capacitors. As shown in the voltage vector V1 of Figure 6, the output voltage vector of Equation (16) is the same, but the balance effect on the charging and discharging of the DC-side capacitor is different.

$$\mathbf{V}_1 = \frac{2}{3}\left(\frac{U_{dc}}{2} + \alpha 0 + \alpha^2 0\right) = \frac{2}{3}\left(0 - \alpha\frac{U_{dc}}{2} - \alpha^2\frac{U_{dc}}{2}\right) = \frac{U_{dc}}{3} \tag{16}$$

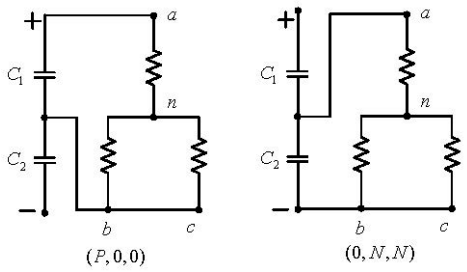


Figure 6. The redundant vectors of V_1.

At the sampling time k, the required output voltage vector is the same, according to Table 1. For example, when (P,0,0) is selected, the midpoint voltage i_N is $-i_a$. When $i_a > 0$, u_{c1} decreases; when $i_a < 0$, u_{c1} increases, and when selecting V_1, $i_a < 0$, if $u_{c1} > u_{c2}$, then select (0, N, N).

Table 1. Redundant switch vector.

Switch State	i_N	$i_x > 0$ $x = a, b, c$	$i_x < 0$ $x = a, b, c$
(P, 0, 0)	$-i_a$	$u_{c1}\downarrow$	$u_{c1}\uparrow$
(0, N, N)	i_a	$u_{c2}\downarrow$	$u_{c2}\uparrow$
(P, P, 0)	i_c	$u_{c1}\uparrow$	$u_{c1}\downarrow$
(0, 0, N)	$-i_c$	$u_{c2}\uparrow$	$u_{c2}\downarrow$
(0, P, 0)	$-i_b$	$u_{c1}\downarrow$	$u_{c1}\uparrow$
(N, 0, N)	i_b	$u_{c2}\downarrow$	$u_{c2}\uparrow$
(0, P, P)	i_a	$u_{c1}\uparrow$	$u_{c1}\downarrow$
(N, 0, 0)	$-i_a$	$u_{c2}\uparrow$	$u_{c2}\downarrow$
(0, 0, P)	$-i_c$	$u_{c1}\downarrow$	$u_{c1}\uparrow$
(N, N,0)	i_c	$u_{c2}\downarrow$	$u_{c2}\uparrow$
(P, 0, P)	i_b	$u_{c1}\uparrow$	$u_{c1}\downarrow$
(0, N, 0)	$-i_b$	$u_{c2}\uparrow$	$u_{c2}\downarrow$

When $u_{c1} \neq u_{c2}$, predict the voltage charging behaviour of the DC-side capacitors C_1 and C_2 and always choose a suitable vector to make the two capacitor voltages more balanced. When making a multi-step prediction, employ the first step: loop 19 voltage

vectors to find the optimal two switching states that make the first step minimise the objective function. If it is a redundant vector, according to the magnitude of u_{c1} and u_{c2}, select the vectors that tend to be equal. In the second step, substitute the two switch states obtained in the first step to obtain the current at the time $k + 1$ and cycle to the previous step. Under the switch state minimised by the objective function, if it is a redundant vector, select the redundant voltage of the capacitor voltage to balance the I vector. The principle diagram of the algorithm is shown in Figure 7.

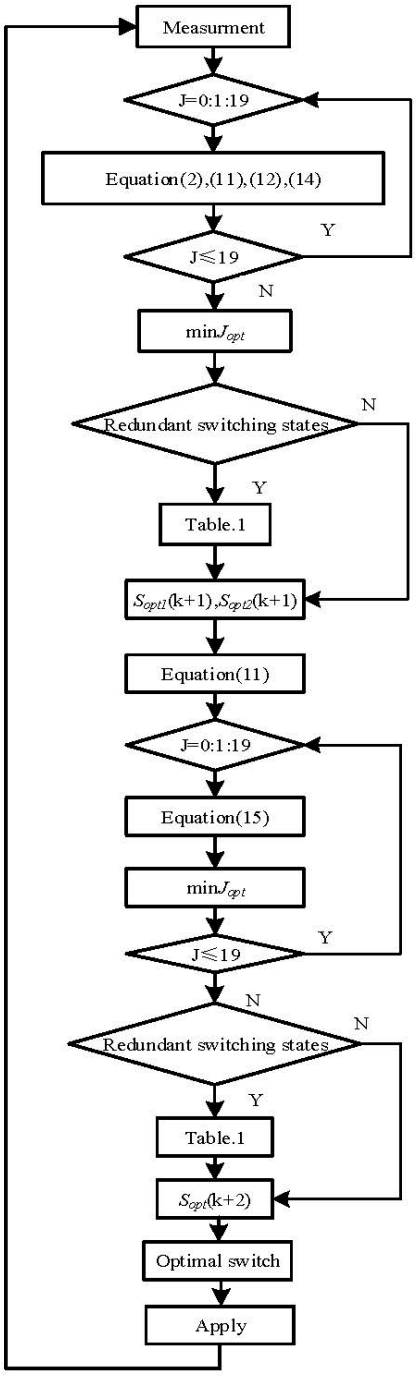


Figure 7. Algorithm implementation principle.

6. Simulation and Results Analysis

Assuming that the three phases are symmetrical, phase A is selected as the analysis object, and the parameters are shown in Table 2.

Table 2. Parameters of the simulation model.

Parameter	Value
Grid voltage and f	380 V, 50 Hz
DC voltage	800 V
Capacitor C_1, C_2	4000 μF
Inductor	2 mH
Resistor	0.01 Ω
Load resistor	8 Ω

Through simulation, the current of the system before the compensation is shown in Figure 8a. The load of the system changes suddenly in 0.4 s. The harmonics detected by the i_p-i_q method are shown in Figure 8b, while Figure 8c shows that the different values of n affect the prediction results of the reference values. Figure 1 shows the predictive results in two different ways. When $n = 2$, the amount of the calculation is small but poor dynamic performance. When $n = 3$, a large amount of calculation is required but excellent dynamic performance is achieved. For the traditional FCS-MPC method, in order to make the tracking current dominant, the following weight factor parameters are set: $\lambda_1 = 0.4$, $\lambda_2 = 0.4$, $\lambda_3 = 0.2$, $\lambda_1 = 0.5$, $\lambda_2 = 0.4$, and $\lambda_3 = 0.1$. However, the method requires a lot of experience, and it is unable to select the optimal weight factor. For the method proposed in this paper, the a-axis and b-axis are equal, $\lambda_1 = \lambda_2 = 0.5$; no other weight factors need to be set.

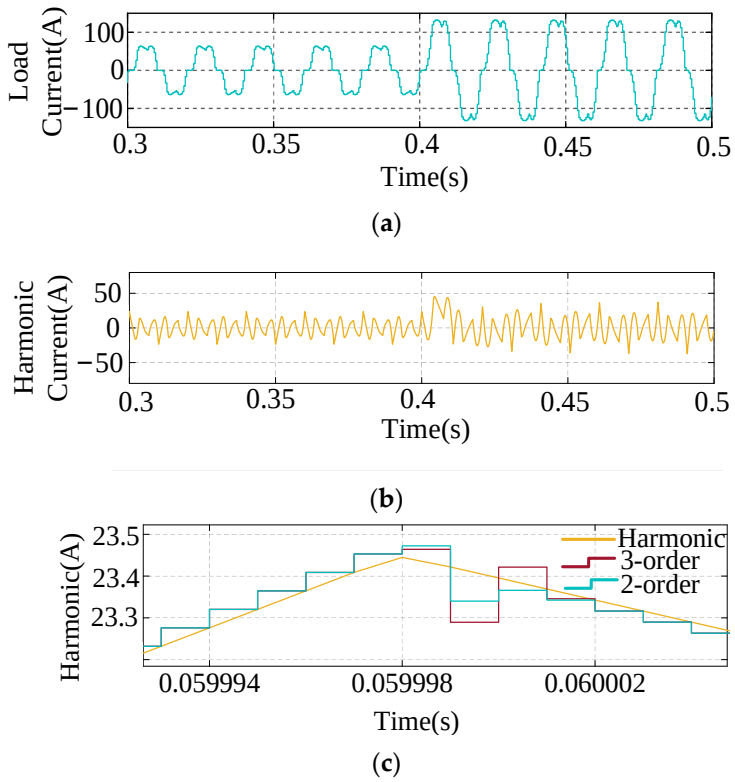


Figure 8. (**a**) Description of the load current with harmonics without compensation. (**b**) Description of the three-phase harmonics detected by the i_p-i_q method in Figure 3. (**c**) Description of the two Lagrange interpolation methods.

When $\lambda_1 = 0.4$, $\lambda_2 = 0.4$, and $\lambda_3 = 0.2$ are selected, the performance of APF as shown in Figure 9a is the compensated grid current, which becomes a sine wave. See Figure 9b for the change of the DC side-voltage when the load changes. The power feedforward method has better dynamic performance. Since the DC-side control method is the same, it is only given in Figure 9. In Figure 9c, the voltages of the capacitors C_1 and C_2 on the DC side can be rebalanced when the load changes. Compared with the other two weighting factors, the balance is better. As shown in Figure 9c,d, the THD (total harmonic distortion) equals 2.13%.

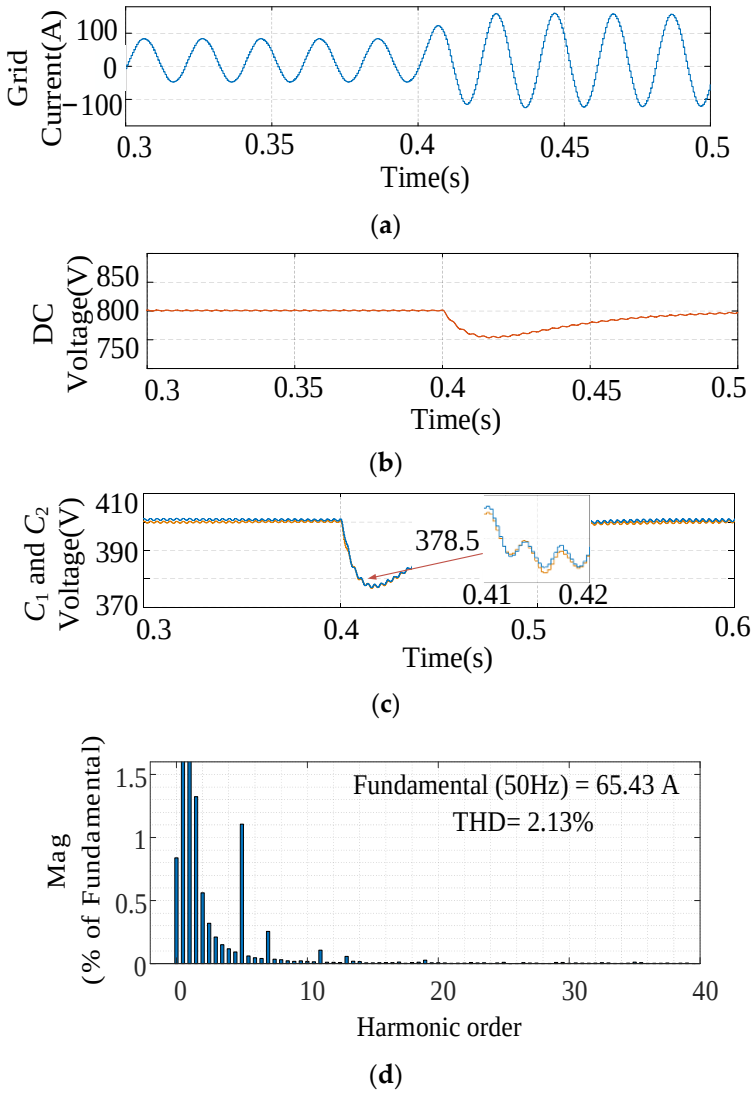


Figure 9. Simulation result when $\lambda_1 = 0.4$, $\lambda_2 = 0.4$, and $\lambda_3 = 0.2$. (**a**) Description of the compensated grid current. (**b**) Description of the Voltage of DC side capacitor. (**c**) Description of the voltage balance of the DC-side capacitors C_1 and C_2. (**d**) Description of the THD rate.

When $\lambda_1 = 0.5$, $\lambda_2 = 0.4$, and $\lambda_3 = 0.1$, as shown in Figure 10a, the compensated grid current is worse than when $\lambda_1 = 0.4$, $\lambda_2 = 0.4$, and $\lambda_3 = 0.2$. In Figure 10b, the voltage balance of the DC-side capacitors C_1 and C_2 is worse than the former, and the THD rate is higher than the former, which is THD = 3.95%.

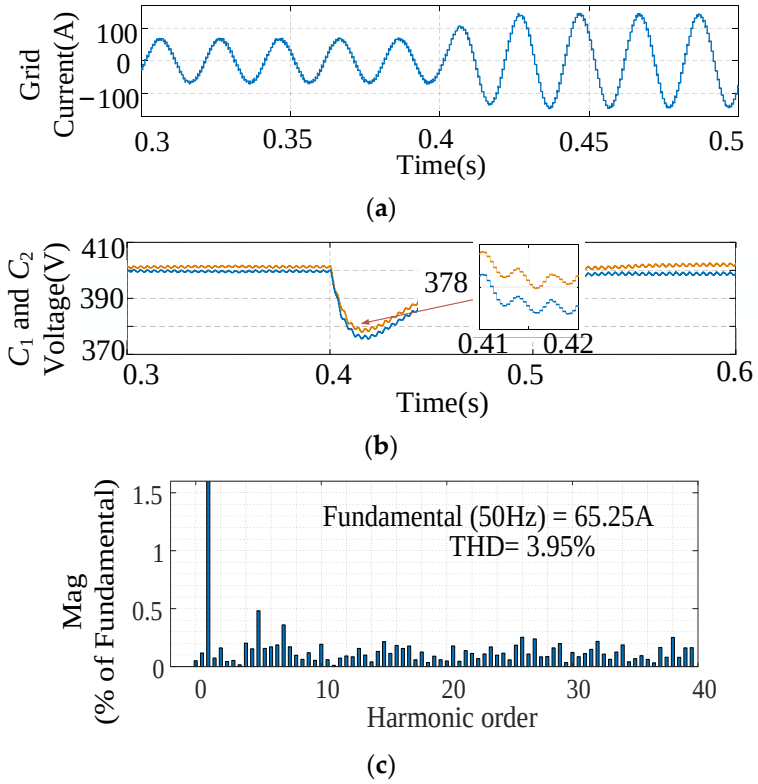


Figure 10. Simulation result when $\lambda_1 = 0.5$, $\lambda_2 = 0.4$, and $\lambda_3 = 0.1$. (**a**) Description of the compensated grid current. (**b**) Description of the voltage balance of the DC-side capacitors C_1 and C_2. (**c**) Description of the THD rate.

The results of the multi-objective single-factor method for multi-step FCS-MPC are shown in Figure 11a as the compensation result, which is a sine wave, and the effect is better than the multi-step multi-objective control method. As seen in Figure 11b, the voltage balance of the DC-side capacitors C_1 and C_2 are slightly worse than when $\lambda_1 = 0.4$, $\lambda_2 = 0.4$, and $\lambda_3 = 0.2$; and better than when $\lambda_1 = 0.5$, $\lambda_2 = 0.4$, and $\lambda_3 = 0.1$; however, the convergence is better. As shown in Figure 11c, the THD = 1.28%.

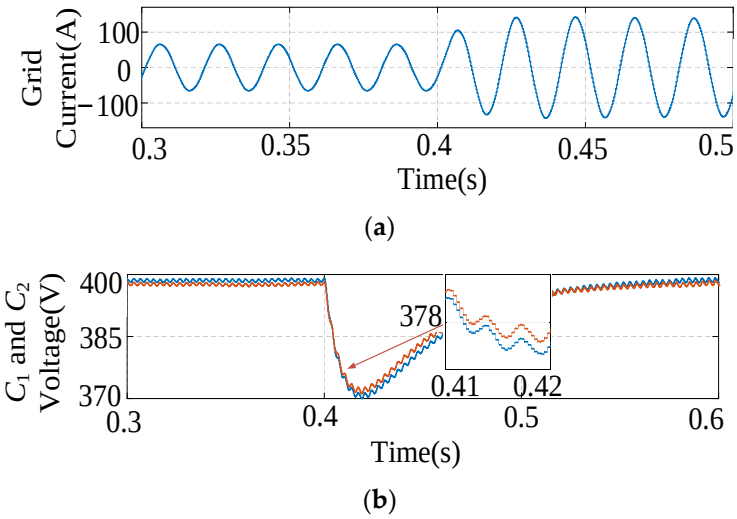
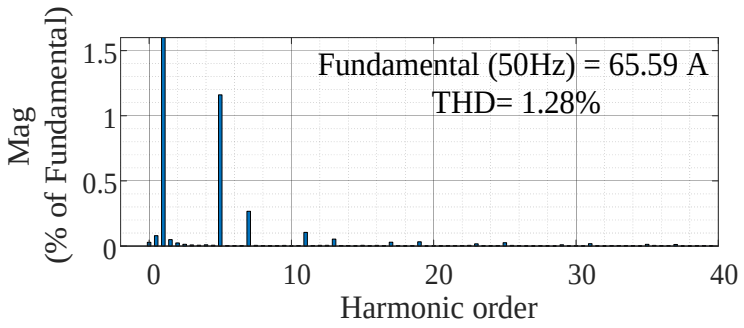


Figure 11. *Cont.*



(**c**)

Figure 11. Single objective method simulation result when $\lambda_1 = \lambda_2 = 0.5$. (**a**) Description of the compensated grid current. (**b**) Description of the voltage balance of the DC-side capacitors C_1 and C_2. (**c**) Description of the THD rate.

The A-phase harmonic changes under the three different weighting factors when the 0.4s load changes are shown in Figure 12. In the single-factor control method, its HTD changes have good stability, and the THD is kept low, which is better than the control method for two different weighting factors under the multi-objective version.

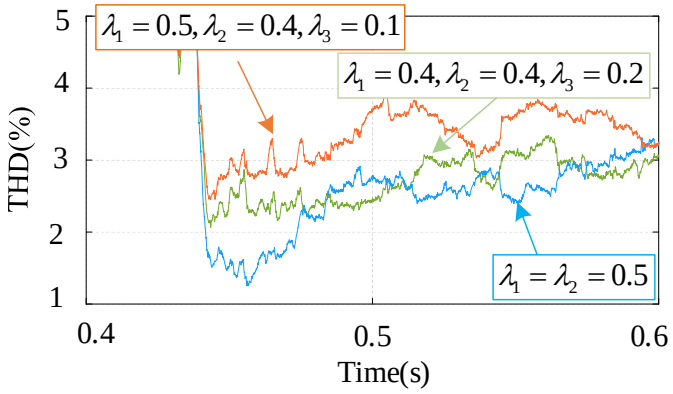


Figure 12. THD dynamic change after load change.

7. Conclusions

This paper presents a method of simplifying the cost function of multi-step FCS-MPC based on multi-level APF. By using the three-level redundant switching characteristics, harmonic reference is completed, and DC side capacitance voltage is balanced, which eliminates the reduction of control effect caused by the selection of the weighting factors. The simplification of the cost function also reduces the calculation amount. The simulation results show that the control method has a good control effect, reduces the harmonic content of the power grid, and meets the standard of the power grid. This method has lower THD than the multi-weighting factor method, which enables the output to follow the reference current, all because the optimal weighted distribution is not needed.

The multi-level structure is closer to the sine wave output, and it lowers the harmonic content, which is the future development trend. The three-level APF single-target multi-step FCS-MPC proposed in this paper is also suitable for AC motors, (Active Front End) AFE, (Static Var Generator) SVG, and so on. It can also be used in a five-level, or even seven-level structure. It reduces the complexity of the vector selection of the multi-level converter and balances the voltage of DC-side capacitance.

Author Contributions: Conceptualization and formal analysis, J.Y.; investigation, H.L.; resources and supervision, J.Y.; validation and writing—original draft preparation., Y.L.; writing—review and editing, Y.L. All authors have read and agreed to the published version of the manuscript.

Funding: Project supported by National Natural Science Foundation of China (NSFC) (61863023).

Institutional Review Board Statement: Not applicable.

Informed Consent Statement: Not applicable.

Data Availability Statement: Not applicable.

Conflicts of Interest: The authors declare no conflict of interest.

References

1. Sinvula, R.; Abo-Al-Ez, K.M.; Kahn, M.T. Total Harmonics Distortion (THD) with PV System Integration in Smart Grids: Case Study. In Proceedings of the 2019 International Conference on the Domestic Use of Energy (DUE), Wellington, South Africa, 25–27 March 2019; pp. 102–108.
2. Xiong, L.; Liu, X.; Liu, Y.; Zhuo, F. Modeling and stability issues of voltage-source converter dominated power systems: A review. *CSEE J. Power Energy Syst.* **2020**. [CrossRef]
3. Garcia-Cerrada, A.; Pinzon-Ardila, O.; Feliu-Batlle, V.; Roncero-Sanchez, P.; Garcia-Gonzalez, P. Application of a Repetitive Controller for a Three-Phase Active Power Filter. *IEEE Trans. Power Electron.* **2007**, *22*, 237–246. [CrossRef]
4. Trinh, Q.-N.; Lee, H.-H. An Advanced Current Control Strategy for Three-Phase Shunt Active Power Filters. *IEEE Trans. Ind. Electron.* **2013**, *60*, 5400–5410. [CrossRef]
5. Daniyal, H.; Lam, E.; Borle, L.J.; Iu, H.H.C. Hysteresis, PI and Ramptime Current Control Techniques for APF: An experimental comparison. In Proceedings of the 2011 6th IEEE Conference on Industrial Electronics and Applications, Beijing, China, 21–23 June 2011; pp. 2151–2156. [CrossRef]
6. Aljohani, T.M.; Ebrahim, A.F.; Mohammed, O. Hybrid Microgrid Energy Management and Control Based on Metaheuristic-Driven Vector-Decoupled Algorithm Considering Intermittent Renewable Sources and Electric Vehicles Charging Lot. *Energies* **2020**, *13*, 3423. [CrossRef]
7. Nagireddy, V.; Kota, V.R.; Kumar, D.A. Hybrid fuzzy back-propagation control scheme for multilevel unified power quality conditioner. *Ain Shams Eng. J.* **2017**, 2709–2724. [CrossRef]
8. Xu, Q.; Ma, F.; Luo, A.; He, Z.; Xiao, H. Analysis and Control of M3C-Based UPQC for Power Quality Improvement in Medium/High-Voltage Power Grid. *IEEE Trans. Power Electron.* **2016**, *31*, 8182–8194. [CrossRef]
9. Kouro, S.; Cortes, P.; Vargas, R.; Ammann, U.; Rodriguez, J. Model Predictive Control—A Simple and Powerful Method to Control Power Converters. *IEEE Trans. Ind. Electron.* **2008**, *56*, 1826–1838. [CrossRef]
10. Rodriguez, J.R.; Kazmierkowski, M.P.; Espinoza, J.R.; Zanchetta, P.; Abu-Rub, H.; Young, H.; Rojas, C.A. State of the Art of Finite Control Set Model Predictive Control in Power Electronics. *IEEE Trans. Ind. Inform.* **2013**, *9*, 1003–1016. [CrossRef]
11. Aguilera, R.P.; Lezana, P.; Quevedo, D.E. Switched Model Predictive Control for Improved Transient and Steady-State Performance. *IEEE Trans. Ind. Inform.* **2015**, *11*, 968–977. [CrossRef]
12. Akagi, H.; Kanazawa, Y.; Nabae, A. Instantaneous Reactive Power Compensators Comprising Switching Devices without Energy Storage Components. *IEEE Trans. Ind. Appl.* **1984**, *IA-20*, 625–630. [CrossRef]
13. Mohapatra, S.R.; Agarwal, V. A Low Computational Cost Model Predictive Controller for Grid Connected Three Phase Four Wire Multilevel Inverter. In Proceedings of the 2018 IEEE 27th International Symposium on Industrial Electronics (ISIE), Cairns, QLD, Australia, 13–15 June 2018; pp. 305–310. [CrossRef]
14. Jin, T.; Shen, X.; Su, T.; Flesch, R.C.C. Model Predictive Voltage Control Based on Finite Control Set With Computation Time Delay Compensation for PV Systems. *IEEE Trans. Energy Convers.* **2018**, *34*, 330–338. [CrossRef]
15. Foster, J.G.L.; Pereira, R.R.; Gonzatti, R.B.; Sant'Ana, W.C.; Mollica, D.; Lambert-Torres, G. A Review of FCS-MPC in Multilevel Converters Applied to Active Power Filters. In Proceedings of the 2019 IEEE 15th Brazilian Power Electronics Conference and 5th IEEE Southern Power Electronics Conference (COBEP/SPEC), Santos, Brazil, 1–4 December 2019; pp. 1–6. [CrossRef]
16. Davari, S.A.; Khaburi, D.A.; Stolze, P.; Kennel, R. An improved Finite Control Set-Model Predictive Control (FCS-MPC) algorithm with imposed optimized weighting factor. In Proceedings of the 2011 14th European Conference on Power Electronics and Applications, Birmingham, UK, 30 August–1 September 2011; pp. 1–10.
17. Narimani, M.; Wu, B.; Yaramasu, V.; Zargari, N.R. Finite Control-Set Model Predictive Control (FCS-MPC) of Nested Neutral Point-Clamped (NNPC) Converter. *IEEE Trans. Power Electron.* **2015**, *30*, 7262–7269. [CrossRef]
18. Vargas, R.; Cortes, P.; Ammann, U.; Rodriguez, J.; Pontt, J. Predictive control of a three-phace ncutral-point-clamped inverter. *IEEE Trans. Ind. Electron* **2007**, *54*, 2697–2705. [CrossRef]
19. Vodyakho, O.; Mi, C.C. Three-Level Inverter-Based Shunt Active Power Filter in Three-Phase Three-Wire and Four-Wire Systems. *IEEE Trans. Power Electron.* **2009**, *24*, 1350–1363. [CrossRef]
20. Barros, J.D.; Silva, J.F. Optimal Predictive Control of Three-Phase NPC Multilevel Converter for Power Quality Applications. *IEEE Trans. Ind. Electron.* **2008**, *55*, 3670–3681. [CrossRef]
21. Xiong, L.; Liu, X.; Liu, Y. Decaying DC and Harmonic Components Detection for Absorbing Impact Load Currents in Weak Grids. *IEEE Trans. Power Deliv.* **2020**, 1. [CrossRef]
22. Li, H.; Liu, Y.; Qi, R.D.; Ding, Y. A novel multi-vector model predictive current control of three-phase active power filter. *Eur. J. Electr. Eng.* **2021**, *23*, 71–78. [CrossRef]